

Localized Patterns in Periodically Forced Systems: II. Patterns with Nonzero Wavenumber*

A. S. Alnahdi[†], J. Niesen[‡], and A. M. Rucklidge[†]

Abstract. In pattern-forming systems, localized patterns are readily found when stable patterns exist at the same parameter values as the stable unpatterned state. Oscillons are spatially localized, time-periodic structures, which have been found experimentally in systems that are driven by a time-periodic force, for example, in the Faraday wave experiment. This paper examines the existence of oscillatory localized states in a PDE model with single-frequency time-dependent forcing, introduced in [A. M. Rucklidge and M. Silber, *SIAM J. Appl. Dyn. Syst.*, 8 (2009), pp. 298–347] as a phenomenological model of the Faraday wave experiment. We choose parameters so that patterns set in with nonzero wavenumber (in contrast to [A. S. Alnahdi, J. Niesen, and A. M. Rucklidge, *SIAM J. Appl. Dyn. Syst.*, 13 (2014), pp. 1311–1327]). In the limit of weak damping, weak detuning, weak forcing, small group velocity, and small amplitude, we reduce the model PDE to the coupled forced complex Ginzburg–Landau equations. We find localized solutions and snaking behavior in the coupled forced complex Ginzburg–Landau equations and relate these to oscillons that we find in the model PDE. Close to onset, the agreement is excellent. The periodic forcing for the PDE and the explicit derivation of the amplitude equations make our work relevant to the experimentally observed oscillons.

Key words. pattern formation, oscillons, localized states, coupled forced complex Ginzburg–Landau equations

AMS subject classifications. 35B36, 35B32, 35Q35, 37L05

DOI. 10.1137/17M1162330

1. Introduction. Spatially localized structures are common in pattern-forming systems, appearing in fluid mechanics, chemical reactions, optics, and granular media [15, 22]. Much progress has been made on the analysis of steady problems, where bistability between a steady pattern and the zero state leads to steady localized patterns bounded by stationary fronts between these two states [9, 14]. In contrast, oscillons, which are oscillating localized structures in a stationary background in periodically forced dissipative systems, are relatively less well understood. Oscillons have been found experimentally in fluid surface wave experiments [5, 19, 24, 25, 35, 40], chemical reactions [31], optical systems [26], and vibrated granular media problems [8, 37, 39]. In the surface wave experiments (see the left panel of Figure 1), the fluid container is driven by vertical vibrations. When these are strong enough, the surface of the system becomes unstable (the Faraday instability) [20], and standing waves are found on the surface of the fluid. Oscillons have been found when this primary bifurcation is subcritical

*Received by the editors December 20, 2017; accepted for publication (in revised form) by M. Book April 5, 2018; published electronically May 22, 2018.

<http://www.siam.org/journals/siads/17-2/M116233.html>

[†]Department of Mathematics & Statistics, College of Science, Al Imam Mohammad Ibn Saud Islamic University, PO Box 240455, Riyadh 11322, KSA (asalahdi@imamu.edu.sa).

[‡]School of Mathematics, University of Leeds, Leeds LS2 9JT, UK (j.niesen@leeds.ac.uk, a.m.rucklidge@leeds.ac.uk).

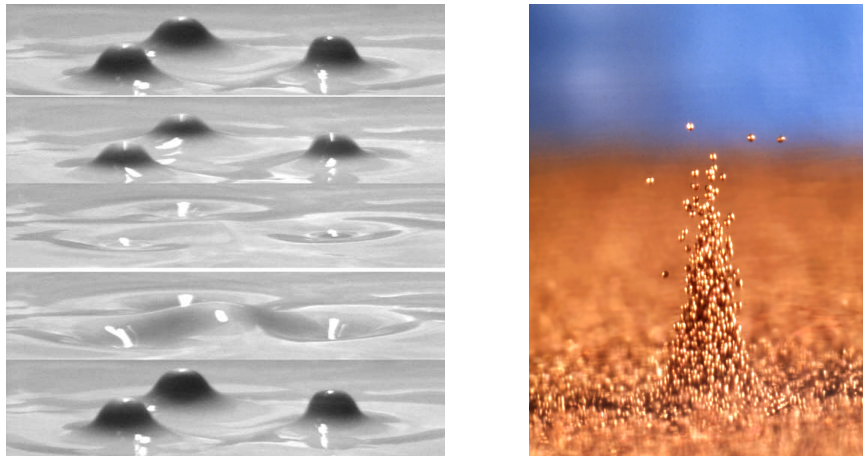


Figure 1. Left: A triad of oscillons in a vertically vibrated colloidal suspension, with time running from top to bottom (taken from [25]). Right: An oscillon in a vertically vibrated layer of bronze beads (courtesy of Paul Umbanhowar, Northwestern University).

[13], and these take the form of alternating conical peaks and craters against a stationary background. A second striking example of oscillons was found in a vertically vibrated thin layer of granular particles [39], as depicted in the right panel of Figure 1. As with the surface wave experiments, oscillons take the shape of alternating peaks and craters. The observation of oscillons in these experiments has motivated our theoretical investigation into the existence of these states and their stability in a model PDE with explicit time-dependent forcing. In both of these experiments, the forcing (vertical vibration) is time-periodic with frequency 2Ω , and the oscillons themselves vibrate either with the same frequency (2Ω) as the forcing (harmonic) or with half the frequency (Ω) of the forcing (subharmonic). We focus on the subharmonic case because this is the most relevant for single-frequency forcing as considered here; in contrast, harmonic oscillations play an important role in the presence of multifrequency forcing [38].

A subharmonic standing wave modulated slowly in time is described by an ansatz of the form

$$(1) \quad U(t, x) = A(T)e^{i\Omega t} \cos(kx) + \text{c.c.}$$

for a real scalar variable U depending on a (fast) time variable t and a spatial variable x . Here, A is a complex amplitude depending on a slow time scale T ; also, k is the wavenumber, and c.c. stands for complex conjugate. Phase shifts in A correspond to translations in time. Symmetry considerations then lead to an amplitude equation of the form

$$(2) \quad A_T = (\rho + i\nu)A + C|A|^2A + i\Gamma\bar{A},$$

where the real parameter Γ describes the strength of the forcing. The parameters ρ and ν are real, but C is complex. The last term (with \bar{A}) breaks the phase symmetry of A and thus the corresponding time-translation symmetry: the phase of A is not arbitrary because the forcing in the original system is time dependent. The factor i in the last term can be removed by applying a phase shift. See [17] for a discussion of this (and related) amplitude equations.

In the case of spatially localized oscillons, we also have to include spatial modulations, so that the amplitude A in (1) depends not only on T but also on a slow spatial variable X . It would seem logical that this ansatz would lead to a diffusion term to (2), yielding a forced complex Ginzburg–Landau (FCGL) equation which is typically written down without derivation [16, 28, 30, 41]:

$$(3) \quad A_T = (\rho + i\nu)A - 2(\alpha + i\beta)A_{XX} + C|A|^2A + i\Gamma\bar{A}.$$

Here, α and β are real parameters; the factor -2 is included for comparison with the results that we will derive in this paper. Burke, Yochelis, and Knobloch [10] showed that this equation admits localized solutions. In [2], the FCGL equation was derived from a model PDE in which patterns are formed with zero wavenumber at onset; the agreement between the localized solutions in the model PDE and those in (3) was excellent.

However, in the Faraday wave experiment, the preferred wavenumber is nonzero at onset [6]. Nevertheless, the FCGL equation has sometimes been used as an amplitude equation for Faraday wave and granular oscillons [4, 16, 37, 42]. In this paper, we argue that this is not appropriate; instead, a system of two coupled FCGL equations should be used, as was done in [27, 33].

In order to demonstrate explicitly the origin and correctness of the coupled FCGL equations as amplitude equations for oscillons, we use a PDE model with single-frequency time-dependent forcing, introduced in [34] as a phenomenological model of the Faraday wave experiment. We simplify the PDE by removing quadratic terms and by taking the parametric forcing to be $\cos(2t)$, where t is the fast time scale. The resulting model PDE is then

$$(4) \quad U_t = (\mu + i\omega)U + (\alpha + i\beta)U_{xx} + (\gamma + i\delta)U_{xxxx} + C|U|^2U + i\operatorname{Re}(U)F\cos(2t),$$

where $U(x, t)$ is a complex function; $\mu < 0$ is the distance from onset of the oscillatory instability; ω , α , β , γ , δ , and F are real parameters; and C is a complex parameter. The $\cos(2t)$ term makes this PDE nonautonomous. In this model, the dispersion relation can be readily controlled so the wavenumber at onset can be chosen to be zero or nonzero, and the nonlinear terms are chosen to be simple in order that the weakly nonlinear theory and numerical solutions can be computed easily. In [2], the wavenumber at the onset of pattern formation was zero, and the FCGL equation was derived as a description of the localized solution. There, we did not require the fourth-order derivatives in (4). In contrast, in the current study we use the dispersion relation to set the wavenumber to be 1 at onset, and therefore we need to retain the term $(\gamma + i\delta)U_{xxxx}$ with the fourth-order spatial derivatives.

Our aim is to find and analyze spatially localized oscillons with nonzero wavenumber in the PDE model (4) theoretically and numerically in one dimension and numerically in two dimensions. The approach will be similar to that in [2], though conceptionally more complicated since we have to consider the interaction between left- and right-traveling waves and the effect of a nonzero group velocity, leading to coupled amplitude equations. Although we will work with a model PDE, our approach will show how localized solutions might be studied in PDEs more directly connected to the Faraday wave experiment, such as the Zhang–Viñals model [43], and how weakly nonlinear calculations from the Navier–Stokes equations [36] might be extended to the oscillons observed in the Faraday wave experiment.

In this case, we can model waves with a slowly varying envelope in one spatial dimension by looking at solutions of the form

$$(5) \quad U(x, t) = A(X, T)e^{i(t+x)} + B(X, T)e^{i(t-x)},$$

where X and T are slow scales and x and t are scaled so that the wave has critical wavenumber $k_c = 1$ and critical frequency $\Omega_c = 1$. Commonly, the complex conjugate is added to an ansatz of the form (5) in order to make U real, but our PDE (4) admits complex solutions (we argue in the conclusion that this does not make a material difference). In order to cover the symmetries of the PDE model, we include both the left- and the right-traveling waves (with amplitudes A and B , respectively), but the time dependence will be e^{it} only, without e^{-it} . In subsection 3.1, we explain in detail how the solution of the linear operator, which we will define later, involves e^{it} only. The $+1$ frequency dominates at leading order because of our choice of dispersion relation. Here, we will focus primarily on the one-dimensional case. Two-dimensional localized oscillons are discussed briefly at the end and studied numerically in more detail in [1].

We start by showing some numerical examples of oscillons in the model PDE (4) and bifurcation diagrams exhibiting snaking, where branches of solutions go back and forth as parameters are varied and the width of the localized pattern increases. We will do an asymptotic reduction of the model PDE to the coupled FCGL equations in the limit of weak damping, weak detuning, weak forcing, small group velocity, and small amplitude, and we will study the properties of the coupled FCGL equations. Some numerical examples of spatially localized oscillons in the coupled FCGL equations will be given. We will also investigate the effect of changing the group velocity. Furthermore, we will reduce the coupled FCGL equations to the real Ginzburg–Landau equation in a further limit of weak forcing and small amplitude close to onset. The real Ginzburg–Landau equation has exact localized sech solutions. Throughout, we will use weakly nonlinear theory by introducing a multiple scale expansion to do the reduction to the amplitude equations. We conclude with numerical examples of strongly localized oscillons in one and two dimensions.

2. Numerical results for the model PDE. Similar to the methodology that was used in [2], we present numerical simulations of the PDE model (4) by time-stepping and continuation. The choice of parameters is guided by the asymptotic analysis in the remainder of the paper: All modes are damped in the absence of forcing, but the modes with wavenumber $k \simeq \pm 1$ are only weakly damped, the forcing is also weak, and the group velocity is small. We discretize the PDE using a Fourier pseudospectral method, and the resulting system of ODEs is solved with a fourth-order exponential time-differencing method [12]. Most experiments are done on a domain of size $L = 120\pi$ (60 wavelengths), in which case we use 2048 grid points. Solving the PDE from an appropriate initial condition, we find the localized solution plotted in the left panel of Figure 2.

To do continuation from this localized solution, we represent solutions by a truncated Fourier series in time with frequencies -3 , -1 , 1 , and 3 . The choice of these frequencies comes from the choice of parameters: The linearized PDE at wavenumber ± 1 looks like $\frac{\partial u}{\partial t} = iu$ (writing $U = u(t)e^{ix}$), so the strongest Fourier component of u looks like e^{it} ; then putting $u = e^{it}$ into the forcing $\text{Re}(e^{it}) \cos(2t)$ generates the frequencies -3 , -1 , 1 , and 3 , as

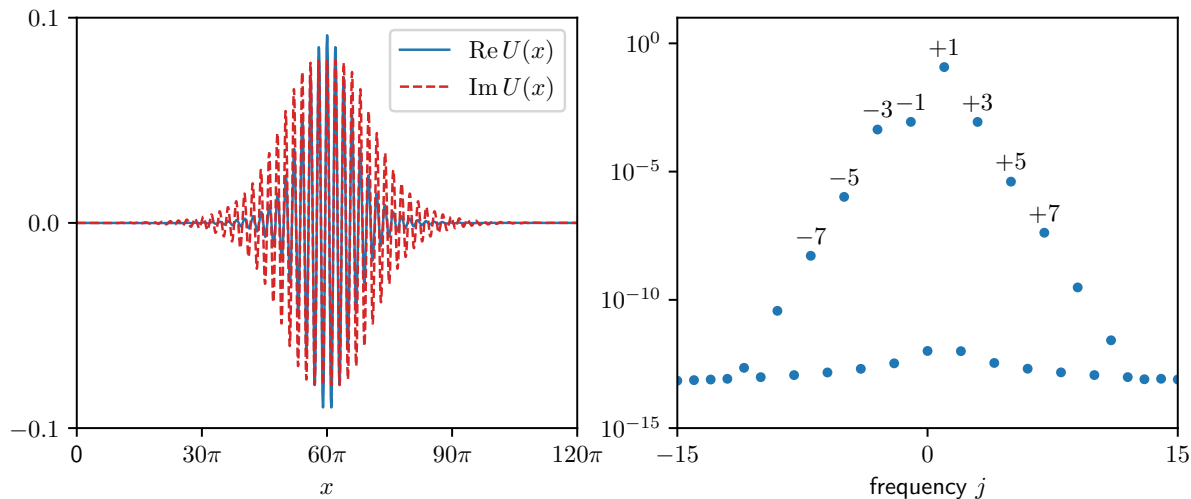


Figure 2. Left: Stable oscillon solution of (4) found by time-stepping, with $\mu = -0.255$, $\omega = 1.5325$, $\alpha = -0.5$, $\beta = 1$, $\gamma = -0.25$, $\delta = 0.4875$, $C = -1 - 2.5i$, and $F = 0.0585$. The solution is plotted at $t = 0$. Right: Amplitude of the e^{ijt} mode with frequency j when expanding the solution in the left panel at $x = 60\pi$ as a Fourier series in time: The frequency $+1$ component is the strongest, followed by frequencies -3 , -1 , and $+3$, as expected, with the other frequencies at least two orders of magnitude weaker.

described in [2]. We also checked numerically that the frequencies ± 1 and ± 3 dominate (see the right panel of Figure 2).

The bifurcation diagram of (4) as computed by AUTO [18] is given in Figure 3. The subcritical transition from the zero state to the pattern occurs at the bifurcation point $F_c = 0.08173$. The saddle-node point where the unstable periodic pattern becomes stable is at $F_d = 0.04811$. The bistability region where we look for the branch of localized states is between F_c and F_d . The branch of localized solutions bifurcates from the branch of periodic patterns at $F_c^* = 0.08056$, which is away from F_c because of the finite domain. Stable localized solutions are located between $F_1 = 0.05666$ and $F_2 = 0.05948$.

Examples of solutions along the branch of localized solutions in Figure 3 are given in Figure 4. Near the point F_c^* where the branch of localized solutions bifurcates, the localized solutions look like the periodic patterns: small amplitude oscillations which are not very localized (see Figure 4(a)). As we go along the branch of localized solutions, the amplitude increases and the unstable oscillons become more localized (Figure 4(b)–(c)). At $F_1 = 0.05695$, the localized oscillons stabilize (Figure 4(d)), and then they lose stability again at $F_2 = 0.05987$ (Figure 4(e)) as the branch of solutions snakes back and forth. The next saddle-node point is at $F_3 = 0.05912$ (Figure 4(f)). It appears from the numerical results that the parameter intervals between successive saddle-node points shrinks to zero as we continue on the branch with localized solutions; this is called *collapsed snaking* in [28]. However, we suspect that our numerics are misleading, partially because the domain size is too small, and that, in fact, the odd and even saddle-node points asymptote to parameter values which are close to each other but not equal. The branch of localized solution connects to the pattern branch close to the saddle-node point F_d . Figure 4(h) shows a typical periodic pattern. All solutions in

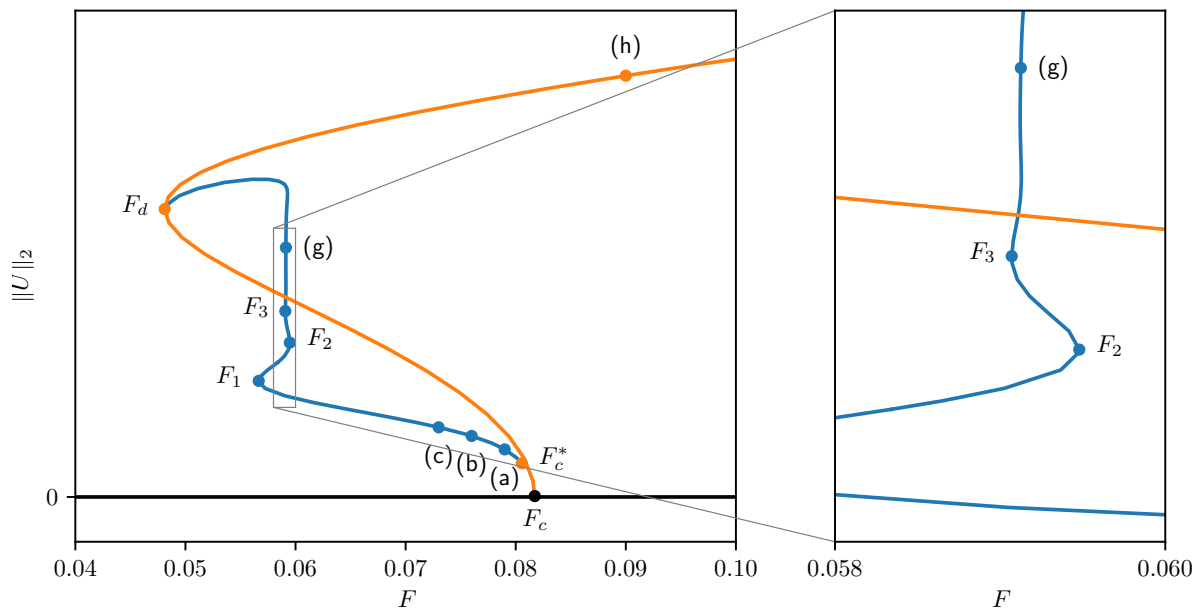


Figure 3. Bifurcation diagram of (4) in the weak damping limit in a domain of size $L_x = 120\pi$ with parameters as in Figure 2. The branch with periodic solutions is plotted in red. The bistability region is between $F_d = 0.04811$ and $F_c = 0.08173$. The branch with localized solutions (blue) starts at $F_c^* = 0.08056$ and has folds at $F_1 = 0.05666$, $F_2 = 0.05948$, and $F_3 = 0.05912$. Solutions at (a), (b), (c), F_1 , F_2 , F_3 , (g), and (h) are shown in Figure 4.

Figures 3 and 4 satisfy $U(x, t) = U(-x, t)$ for a suitably chosen origin. We have not found solutions with any other symmetry.

In the remainder of the paper, we will analyze these oscillons and derive an asymptotic expression for their amplitude, which will be compared to the numerical solutions in Figure 9.

3. Derivation of the coupled FCGL equation. In this section, we will study the PDE model (4) in the limit of weak damping, weak detuning, weak forcing, and small amplitude in order to derive its amplitude equation. In addition, we will need to assume that the group velocity is small. We start with linearizing (4) about zero, and we consider solutions of the form $U(x, t) = e^{\sigma t + ikx}$, where σ is the complex growth rate of a mode with wavenumber k . Without taking any limits and without considering the forcing, the growth rate is given by

$$(6) \quad \sigma = \mu - \alpha k^2 + \gamma k^4 + i(\omega - \beta k^2 + \delta k^4),$$

so $\sigma_r = \mu - \alpha k^2 + \gamma k^4$ gives the damping rate of modes with wavenumber k , and $\sigma_i = \omega - \beta k^2 + \delta k^4$ gives the frequency of oscillation. We will also need the group velocity of the waves, which is $d\sigma_i(k)/dk = -2\beta k + 4\delta k^3$.

We will choose parameters so that we are in a weak damping, weak detuning, and small group velocity limit for modes with wavenumber $k = 1$. Specifically, in order to find spatially localized oscillons and to do the reduction to the amplitude equation, we will impose the following.

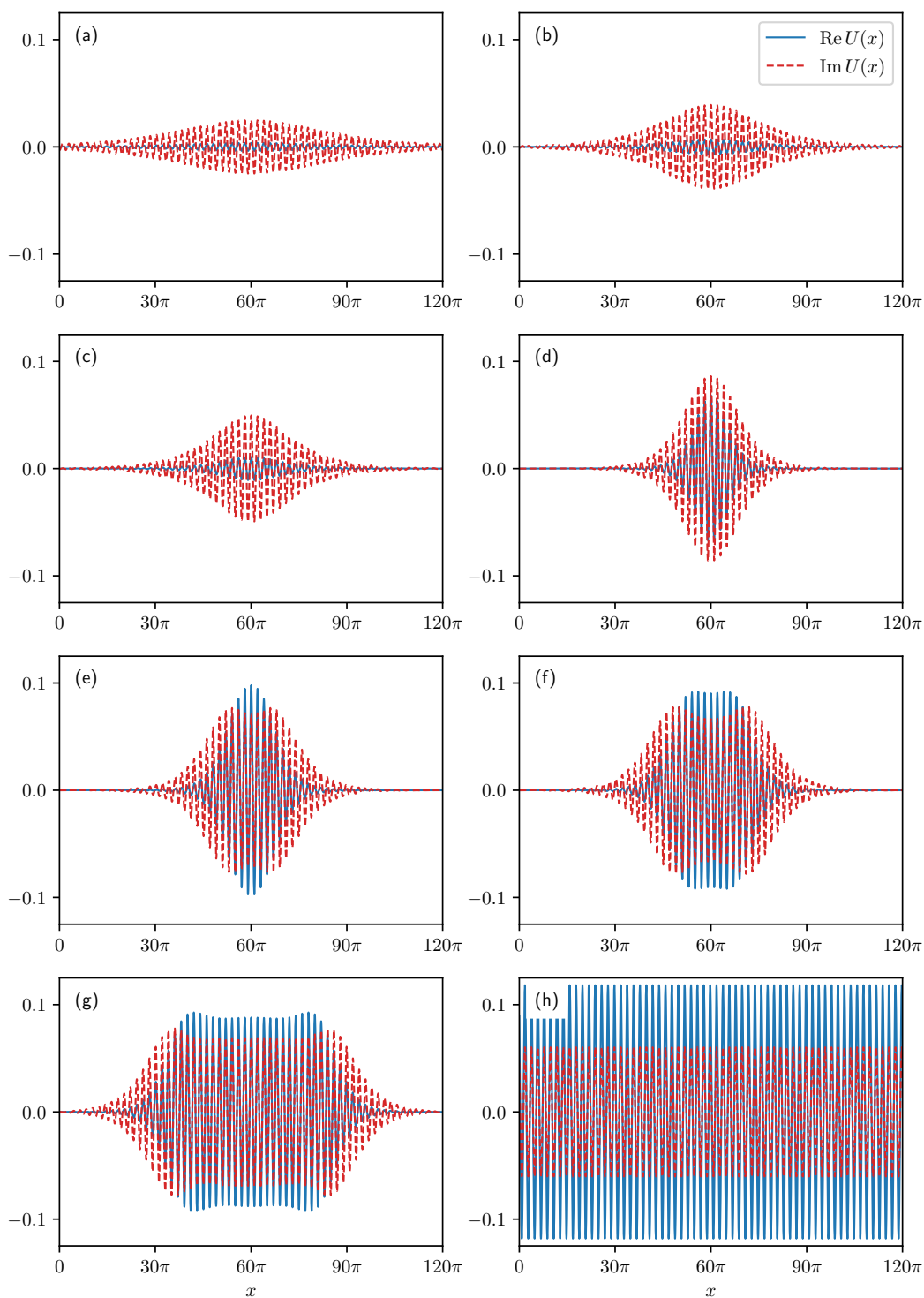


Figure 4. Solutions along the branch of localized solutions in the bifurcation diagram in Figure 3 at (a) $F = 0.079$, (b) $F = 0.076$, (c) $F = 0.073$, (d) the fold at $F_1 = 0.05666$, (e) the fold at $F_2 = 0.05948$, (f) the fold at $F_3 = 0.05912$, and the point (g). Solution (h) is on the periodic branch at $F = 0.09$.

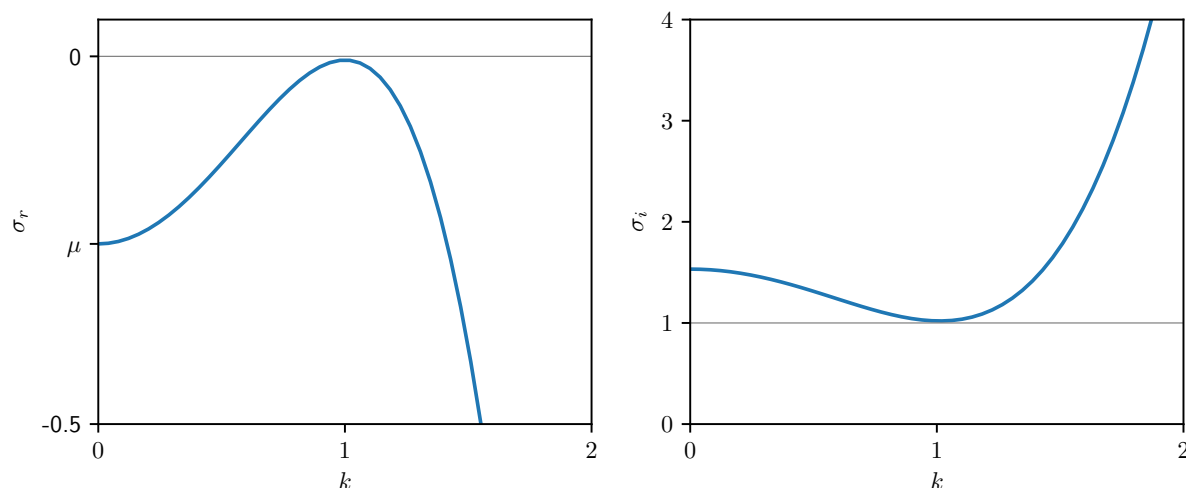


Figure 5. The growth rate (left panel) and dispersion relation (right panel) of (4) with $\mu = -0.255$, $\omega = 1.5325$, $\alpha = -0.5$, $\beta = 1$, $\gamma = -0.25$, and $\delta = 0.4875$. In this case, the group velocity is small at $k = 1$ because this is close to the minimum of the dispersion relation.

Stability in the absence of forcing. To have waves with all wavenumbers linearly damped, we require that $\sigma_r(k) < 0$ for all k . It follows that $\mu < 0$, $\alpha > -2\sqrt{\mu\gamma}$, and $\gamma < 0$. With $\alpha < 0$, we have a nonmonotonic growth rate.

Preferred wavenumber. We want the damping to be weakest for $k = \pm 1$. Thus, we require that the growth rate σ_r achieves a maximum when the wavenumber k is 1, so $\frac{d}{dk}\sigma_r(k=1) = -2\alpha + 4\gamma = 0$. This gives the condition $\alpha = 2\gamma$.

Weak damping. We also need to make the growth rate σ_r be close to zero when $k = \pm 1$. Therefore, we introduce a small parameter $\epsilon \ll 1$ and a new parameter ρ , so that we have $\sigma_r(k=1) = \mu - \alpha + \gamma = \epsilon^2\rho$, where $\rho < 0$. Thus, $\mu = \frac{1}{2}\alpha + \epsilon^2\rho$. Figure 5(a) shows an example of the real part of the growth rate.

Weak detuning. We want waves with $k \simeq \pm 1$ to be subharmonically driven by $\cos(2t)$, so the frequency of the oscillation σ_i should be close to 1 at $k = 1$. Therefore, we write $\sigma_i(k=1) = \omega - \beta + \delta = 1 + \epsilon^2\nu$, where ν is the detuning.

Small group velocity. We require the group velocity $\frac{d\sigma_i}{dk} = -2k\beta + 4\delta k^3$ to be $O(\epsilon)$ at $k = \pm 1$, so we have $-2\beta + 4\delta = \epsilon\nu_g$. This is needed to allow the group velocity in the subsequent amplitude equations to appear at the same order as all the other terms. We discuss the consequences of choosing a small group velocity in section 6. Figure 5(b) shows an example of the dispersion relation $\sigma_i(k)$.

Weak forcing. To perform the weakly nonlinear theory, we assume that the forcing is weak, and so we scale the forcing amplitude to be $O(\epsilon^2)$, writing $F = 4\epsilon^2\Gamma$.

We relate the parameters in the PDE model with the parameters in the amplitude equations in a way that we can connect examples of localized oscillons in both equations. In Table 1, all PDE parameters are defined in terms of parameters that will appear in the coupled FCGL equations and vice versa.

Table 1

Relationships between parameters $(\mu, \omega, \alpha, \beta, \gamma, \delta, F)$ of the PDE model and the parameters $(\rho, \nu, \alpha, \beta, v_g, \Gamma)$ of the coupled FCGL equations. Note that these relationships depend on the choice of ϵ . The parameters α and β are the same in both models.

The PDE model (4)	The coupled FCGL (14)	Physical meaning
$\mu = \alpha - \gamma + \epsilon^2 \rho = \frac{1}{2}\alpha + \epsilon^2 \rho$ $\gamma = \frac{1}{2}\alpha$	$\rho = \frac{\mu - \alpha + \gamma}{\epsilon^2}$	$\rho = \text{damping } (\rho < 0)$
$\delta = \frac{1}{2}\beta + \frac{1}{4}\epsilon v_g$	$v_g = \frac{-2\beta + 4\delta}{\epsilon}$	$v_g = \text{group velocity}$
$\omega = 1 + \frac{1}{2}\beta - \frac{1}{4}\epsilon v_g + \epsilon^2 \nu$	$\nu = \frac{\omega - 1 - \frac{\beta}{2} + \delta}{\epsilon^2}$	$\nu = \text{detuning}$
$F = 4\epsilon^2 \Gamma$	$\Gamma = \frac{F}{4\epsilon^2}$	$\Gamma = \text{strength of parametric forcing}$

3.1. Linear theory. With the parameters as in Table 1, the linear theory of the PDE (4) at leading order is given by

$$(7) \quad U_t = \left(\frac{\alpha}{2} + i \left(\frac{\beta}{2} + 1 \right) \right) U + (\alpha + i\beta) U_{xx} + \left(\frac{\alpha}{2} + i \frac{\beta}{2} \right) U_{xxxx},$$

which defines a linear operator L as

$$LU = \left(-\frac{\partial}{\partial t} + i \right) U + \left(\frac{\alpha}{2} + i \frac{\beta}{2} \right) \left(1 + \frac{\partial^2}{\partial x^2} \right)^2 U.$$

This is essentially the linear part of the complex Swift–Hohenberg equation [3], which has appeared in the context of nonlinear optics [23] and Taylor–Couette flows [7]. To find all solutions, we substitute $U = e^{\sigma t + ikx}$ into the above equation to get the dispersion relation

$$\sigma = i + \left(\frac{\alpha}{2} + i \frac{\beta}{2} \right) (1 - k^2)^2.$$

We assume that our problem has periodic boundary conditions, which implies that $k \in \mathbb{R}$. Furthermore, we require $\sigma_r = 0$ since we are considering neutral modes. The real and imaginary parts of this equation give

$$k = \pm 1 \quad \text{and} \quad \sigma = i.$$

Therefore, $LU = 0$, equivalent to (7), implies that neutral modes are linear combinations of $U(x, t) = e^{i(t+x)}$ and $U(x, t) = e^{i(t-x)}$. Note that our choice of dispersion relation leads to positive frequency solutions. This is not a severe restriction, as discussed in section 6.

3.2. Weakly nonlinear theory. In order to apply the standard weakly nonlinear theory, we need the adjoint linear operator L^\dagger . Therefore, we define an inner product between two functions $f(x, t)$ and $g(x, t)$ by

$$(8) \quad \langle f(x, t), g(x, t) \rangle = \frac{1}{4\pi^2} \int_0^{2\pi} \int_0^{2\pi} \bar{f}(x, t)g(x, t) dt dx,$$

where \bar{f} is the complex conjugate of f . The adjoint linear operator L^\dagger is defined by the relation

$$\langle f(x, t), Lg(x, t) \rangle = \langle L^\dagger f(x, t), g(x, t) \rangle \quad \text{for all } f \text{ and } g,$$

and so, using integration by parts,

$$L^\dagger f = \left(\frac{\partial}{\partial t} - i + \left(\frac{\alpha}{2} - i\frac{\beta}{2} \right) \left(1 + \frac{\partial^2}{\partial x^2} \right)^2 \right) f.$$

Taking the adjoint changes the sign of the $\frac{\partial}{\partial t}$ term and takes the complex conjugate of other terms of L . The adjoint eigenfunctions are then given by solving $L^\dagger f = 0$; the solutions are also linear combinations of $e^{i(t \pm x)}$.

We expand U in powers of the small parameter ϵ :

$$(9) \quad U = \epsilon U_1 + \epsilon^2 U_2 + \epsilon^3 U_3 + \dots,$$

where U_1, U_2, U_3, \dots are $O(1)$ complex functions. We will derive solutions U_1, U_2, U_3, \dots at each order of ϵ .

At $O(\epsilon)$, the linear theory arises, and we find $LU_1 = 0$. The solution U_1 takes the form

$$(10) \quad U_1 = A(X, T)e^{i(t+x)} + B(X, T)e^{i(t-x)},$$

where A and B represent the amplitudes of the left- and right-traveling waves. They are functions of X and T , the long and slow scale modulations of space and time variables:

$$T = \epsilon^2 t \quad \text{and} \quad X = \epsilon x.$$

The multiple scale expansion below will determine the evolution equations for $A(X, T)$ and $B(X, T)$.

At second order in ϵ , we get $LU_2 = 0$: The $\frac{\partial^2 U_1}{\partial x \partial X}$ term cancels with the $\frac{\partial^4 U_1}{\partial x^3 \partial X}$ term. We would have had a forcing term at this order if we had not ensured that the group velocity is $O(\epsilon)$. The equation at this order is solved by setting $U_2 = 0$.

At third order in ϵ , we get

$$(11) \quad \begin{aligned} \frac{\partial U_1}{\partial T} = & LU_3 + (\rho + i\nu)U_1 + (\alpha + i\beta)\frac{\partial^2 U_1}{\partial X^2} + 3(\alpha + i\beta)\frac{\partial^4 U_1}{\partial x^2 \partial X^2} \\ & + i\nu_g \frac{\partial^4 U_1}{\partial x^3 \partial X} + 4i\Gamma \cos(2t) \operatorname{Re}(U_1) + C|U_1|^2 U_1. \end{aligned}$$

The linear operator L is singular, so we must apply a solvability condition: We take the inner product between the adjoint eigenfunction $e^{i(t+x)}$ and (11), which gives

$$(12) \quad \begin{aligned} \left\langle e^{i(t+x)}, \frac{\partial U_1}{\partial T} \right\rangle = & \left\langle e^{i(t+x)}, LU_3 \right\rangle + (\rho + i\nu) \left\langle e^{i(t+x)}, U_1 \right\rangle + (\alpha + i\beta) \left\langle e^{i(t+x)}, \frac{\partial^2 U_1}{\partial X^2} \right\rangle \\ & + 3(\alpha + i\beta) \left\langle e^{i(t+x)}, \frac{\partial^4 U_1}{\partial x^2 \partial X^2} \right\rangle + i\nu_g \left\langle e^{i(t+x)}, \frac{\partial^4 U_1}{\partial x^3 \partial X} \right\rangle \\ & + 4i\Gamma \left\langle e^{i(t+x)}, \cos(2t) \operatorname{Re}(U_1) \right\rangle + C \left\langle e^{i(t+x)}, |U_1|^2 U_1 \right\rangle. \end{aligned}$$

We have $\langle e^{i(t+x)}, LU_3 \rangle = \langle L^\dagger e^{i(t+x)}, U_3 \rangle = 0$, so U_3 is removed, and the above equation becomes an equation in U_1 only. Substituting the solution U_1 leads to

$$\begin{aligned}
 & \left\langle e^{i(t+x)}, \frac{\partial}{\partial T} (Ae^{i(t+x)} + Be^{i(t-x)}) \right\rangle \\
 &= (\rho + i\nu) \left\langle e^{i(t+x)}, Ae^{i(t+x)} + Be^{i(t-x)} \right\rangle \\
 &+ (\alpha + i\beta) \left\langle e^{i(t+x)}, \frac{\partial^2}{\partial X^2} (Ae^{i(t+x)} + Be^{i(t-x)}) \right\rangle \\
 (13) \quad &+ 3(\alpha + i\beta) \left\langle e^{i(t+x)}, \frac{\partial^4}{\partial x^2 \partial X^2} (Ae^{i(t+x)} + Be^{i(t-x)}) \right\rangle \\
 &+ iv_g \left\langle e^{i(t+x)}, \frac{\partial^4}{\partial x^3 \partial X} (Ae^{i(t+x)} + Be^{i(t-x)}) \right\rangle \\
 &+ 4i\Gamma \left\langle e^{i(t+x)}, \frac{1}{2} \cos(2t) (Ae^{i(x+t)} + Be^{i(t-x)} + \bar{A}e^{-i(t+x)} + \bar{B}e^{-i(t-x)}) \right\rangle \\
 &+ C \left\langle e^{i(t+x)}, (|A|^2 + A\bar{B}e^{2ix} + \bar{A}Be^{-2ix} + |B|^2) (Ae^{i(t+x)} + Be^{i(t-x)}) \right\rangle.
 \end{aligned}$$

After we compute the left- and right-hand sides of the above equation term by term, we get equations for the amplitudes $A(X, T)$ and $B(X, T)$:

$$\begin{aligned}
 (14) \quad & \frac{\partial A}{\partial T} = (\rho + i\nu)A - 2(\alpha + i\beta) \frac{\partial^2 A}{\partial X^2} + v_g \frac{\partial A}{\partial X} + C(|A|^2 + 2|B|^2)A + i\Gamma \bar{B}, \\
 & \frac{\partial B}{\partial T} = (\rho + i\nu)B - 2(\alpha + i\beta) \frac{\partial^2 B}{\partial X^2} - v_g \frac{\partial B}{\partial X} + C(2|A|^2 + |B|^2)B + i\Gamma \bar{A}.
 \end{aligned}$$

Thus, the PDE model has been reduced to the coupled FCGL equations in the weak damping, weak detuning, small group velocity, and small amplitude limit. In (14), the group velocity terms have different signs, which makes the envelopes travel in opposite directions. The $-2\alpha \frac{\partial^2 A}{\partial X^2}$ may make the above equations look like they are ill posed, but recall that $\alpha < 0$.

4. Properties of the coupled FCGL equations. Following [21], we can identify the symmetries and how they affect the structure of (14). The original system is invariant under translations in x : Replacing x by $x + \phi^*$, where ϕ^* is arbitrary, we get

$$U(x + \phi^*, t) = A(X + \epsilon\phi^*, T) e^{i(t+x+\phi^*)} + B(X + \epsilon\phi^*, T) e^{i(t-x-\phi^*)},$$

which is also a solution of the problem. This translation has the effect of shifting X to $X + \epsilon\phi^*$ and changing the phase of A and B : If we suppress the change from X to $X + \epsilon\phi^*$, then (14) is equivariant under

$$A \rightarrow Ae^{i\phi^*}, \quad B \rightarrow Be^{-i\phi^*},$$

which is therefore a symmetry of (14). Equations (14) are also invariant under translations in X , but this is an artifact of the truncation at cubic order [29]. Similarly, we can reflect in x , which leads to the symmetry $A \leftrightarrow B$, $\partial_x \leftrightarrow -\partial_x$.

Amplitude equations associated with a Hopf bifurcation (a weakly damped Hopf bifurcation in this case) usually have time translation symmetry, which manifests as equivariance

under phase shifts of the amplitudes. However, the underlying PDE is nonautonomous, and so rotating A and B by a common phase is not a symmetry of (14). Equations (14) do possess T -translation symmetry, but this is also an artifact.

The parametric forcing provides an interesting coupling between the left- and right-traveling waves with amplitudes A and B , which means that solutions or symmetries that one might expect at first glance are in fact not present. For example, the coupling terms in the coupled FCGL equations make it impossible to find pure traveling waves; i.e., $A \neq 0, B = 0$ is not a solution of (14). Also, solutions with $A = B$ exist only if v_g is zero, which generically it is not. Finally, steady standing wave solutions (which are typically seen in Faraday wave experiments) have $B(X) = A(-X)$; substituting this into (14) yields a nonlocal equation that is not a PDE, though all solutions we present in this paper are in this category.

4.1. The zero solution. The stability of the zero state under small perturbations with complex growth rate s and real wavenumber q can be studied by linearizing (14), writing A and B as

$$A = \hat{A}e^{sT+iqX} \quad \text{and} \quad B = \hat{B}e^{\bar{s}T-iqX},$$

where $|\hat{A}| \ll 1, |\hat{B}| \ll 1$, and $\hat{A}, \hat{B} \in \mathbb{C}$. We choose $\hat{B}e^{\bar{s}T-iqX}$ in order that the exponential term will cancel in the next step. Substituting this into (14), linearizing, and taking the complex conjugate of the second equation gives

$$\begin{aligned} s\hat{A} &= (\rho + i\nu)\hat{A} + 2(\alpha + i\beta)q^2\hat{A} + iv_gq\hat{A} + i\Gamma\bar{\hat{B}}, \\ s\bar{\hat{B}} &= (\rho - i\nu)\bar{\hat{B}} + 2(\alpha - i\beta)q^2\bar{\hat{B}} - iv_gq\bar{\hat{B}} - i\Gamma\hat{A}. \end{aligned} \tag{15}$$

This is a linear homogeneous system of equations, so there is a nontrivial solution only when its determinant is zero. The imaginary part of the determinant equals $2s_i(\rho + 2\alpha q^2 - s_r)$, where s_r and s_i denote the real and imaginary part of s . We are interested in locating the bifurcation where zero solution is neutrally stable, so $s_r = 0$. Since ρ and α are negative, the determinant can only be zero if $s_i = 0$. Thus, there is no Hopf bifurcation, and the neutral stability condition is $s = 0$. Setting the real part of the determinant of (15) equal to zero leads to

$$(\rho + 2\alpha q^2)^2 + (\nu + 2\beta q^2 + v_g q)^2 = \Gamma^2. \tag{16}$$

The stability of the zero state changes when $\Gamma = \Gamma_c$, the minimum of the neutral stability curve, and the nonzero flat state is created with $q = q_c$. This corresponds to a uniform pattern in the PDE (4) with wavenumber $k_c = 1 + \epsilon q_c$. The critical wavenumber q_c can be computed by minimizing the left-hand side of (16). Differentiating with respect to q yields the following cubic equation in q :

$$4\alpha q(\rho + 2\alpha q^2) + (4\beta q + v_g)(\nu + 2\beta q^2 + v_g q) = 0. \tag{17}$$

Solving this gives q_c , the critical wavenumber, which is positive if $\nu v_g < 0$ and negative if $\nu v_g > 0$. Substituting $q = q_c$ into (16) gives Γ_c .

4.2. Standing waves. Now we look at steady equal-amplitude states of the form $A = R_0 e^{i(qX + \phi_1)}$ and $B = R_0 e^{i(-qX + \phi_2)}$, where R_0 and q are real and ϕ_1 and ϕ_2 are the phases. These represent uniform standing wave patterns with wavenumber $1 + \epsilon q$ in $U(x)$. We substitute this into (14), which yields, assuming that R_0 is not zero,

$$0 = (\rho + i\nu) + 2(\alpha + i\beta)q^2 + iv_g q + 3CR_0^2 + i\Gamma e^{-i\Phi},$$

where $\Phi = \phi_1 + \phi_2$. This is the same equation obtained for steady constant-amplitude solutions of the single FCGL equation (3) but with a group velocity term. The real and imaginary parts of the above equation are

$$(18) \quad \begin{aligned} \text{Re: } 0 &= \rho + 2\alpha q^2 + 3C_r R_0^2 + \Gamma \sin \Phi, \\ \text{Im: } 0 &= \nu + 2\beta q^2 + v_g q + 3C_i R_0^2 + \Gamma \cos \Phi. \end{aligned}$$

We eliminate Φ by using the identity $\cos^2 \Phi + \sin^2 \Phi = 1$ to give the following polynomial equation for R_0 :

$$(19) \quad \begin{aligned} 0 &= 9(C_r^2 + C_i^2)R_0^4 + 6((\rho + 2\alpha q^2)C_r + (\nu + v_g q + 2\beta q^2)C_i)R_0^2 \\ &\quad + (\rho + 2\alpha q^2)^2 + (\nu + v_g q + 2\beta q^2)^2 - \Gamma^2. \end{aligned}$$

This is a quadratic equation in R_0^2 , and its discriminant is given by

$$\begin{aligned} \Delta &= 36((\rho + 2\alpha q^2)C_r + (\nu + v_g q + 2\beta q^2)C_i)^2 \\ &\quad - 36((\rho + 2\alpha q^2)^2 + (\nu + v_g q + 2\beta q^2)^2 - \Gamma^2)(C_r^2 + C_i^2). \end{aligned}$$

Examination of the polynomial (19) shows that when the forcing amplitude Γ reaches $((\rho + 2\alpha q^2)^2 + (\nu + v_g q + 2\beta q^2)^2)^{1/2}$, a subcritical bifurcation occurs provided that $(\rho + 2\alpha q^2)C_r + (\nu + v_g q + 2\beta q^2)C_i < 0$. Spatially oscillatory states A_{sp}^- and B_{sp}^- are created, which turn into A_{sp}^+ and B_{sp}^+ states at a saddle-node ($\Delta = 0$) bifurcation at $\Gamma = \Gamma_d$, with

$$(20) \quad \Gamma_d = \sqrt{(\rho + 2\alpha q^2)^2 + (\nu + v_g q + 2\beta q^2)^2 - \frac{((\rho + 2\alpha q^2)C_r + (\nu + v_g q + 2\beta q^2)C_i)^2}{C_r^2 + C_i^2}}.$$

Figure 6 shows (16) and (20) in the (ν, Γ) parameter plane, where we have taken $q = q_c$ from (17). The values of the parameters ρ , α , β , v_g , C_r , and C_i in the figure correspond to the parameters in the figures in section 2 with $\epsilon = 0.1$. The primary bifurcation changes from supercritical to subcritical when $(\rho + 2\alpha q^2)C_r + (\nu + v_g q + 2\beta q^2)C_i = 0$, which is at $\nu = 0.2228$ for the parameter values in Figure 6. Localized solutions can be found in the bistability region between Γ_c and Γ_d .

4.3. Localized solutions. In order to find localized solutions of the coupled FCGL equations (14), one might attempt an ansatz of the form

$$A = R_0(X, T) e^{i(qX + \phi_1)} \quad \text{and} \quad B = \bar{R}_0(X, T) e^{i(-qX + \phi_2)}$$

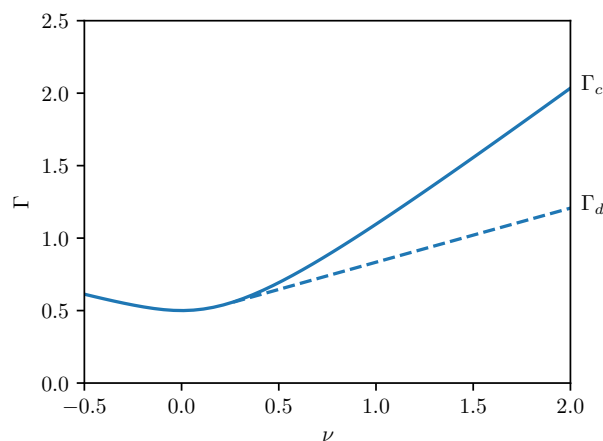


Figure 6. The (ν, Γ) parameter plane of the coupled FCGL equations (14) with $\rho = -0.5$, $\alpha = -0.5$, $\beta = 1$, $v_g = -0.5$, and $C = -1 - 2.5i$. These parameters with $\epsilon = 0.1$ correspond to the parameters of the model PDE (4) used in the figures in section 2. The solid line shows the primary pitchfork bifurcation at Γ_c , where the zero state becomes unstable to perturbations with wavenumber q_c . The dash line shows the saddle-node bifurcation at Γ_d .

with R_0 complex and q, ϕ_1, ϕ_2 real. This is a spatially modulated version of the standing wave studied in the previous section. However, the coupled FCGL equations admit no solution of this form, even if $v_g = 0$. Other standing wave ansatzes are possible, e.g., $A = R_0(X) e^{i(qX + \phi_1)}$ and $B = \bar{R}_0(-X) e^{i(-qX + \phi_2)}$, but we have not explored these further.

We were able to find analytic expressions for localized solutions of the coupled FCGL equations by taking further asymptotic limits (see section 5). To motivate the subsequent calculations, we present some numerical examples of stable spatially localized oscillons in the coupled FCGL equations found by using the same numerical method as in section 2 on a periodic domain of size 20π . We take the same parameter values as before: $\rho = -0.5$, $\nu = 2$, $\alpha = -0.5$, $\beta = 1$, and $C = -1 - 2.5i$.

The top row of Figure 7 shows an example of a localized oscillon in the coupled FCGL equations with $v_g = -0.2$. As we increase the magnitude of the group velocity v_g to $v_g = -0.5$ (second row) and $v_g = -1$ (third row) and change the forcing strength Γ so that we are still in the region where the localized solution is stable, we can see that A and B start to move apart, pulled in opposite directions by the group velocity term. We can use these solutions to the coupled FCGL equations to reconstruct first-order approximations to solutions of the PDE model (4) with the help of (9) and (10); this is shown in the bottom row of Figure 7.

We also computed the bifurcation diagram of the coupled FCGL equations on a domain of size 20π using AUTO [18]. The critical wavenumber with the above parameter values is $q_c = 0.09950 \approx \frac{1}{10}$, so the periodic solution fits almost perfectly in this domain. The result is shown in Figure 8. The branch of periodic solution bifurcates from the zero solution at $\Gamma_c = 2.035$ and has a fold at $\Gamma_d = 1.206$. Using the relation $F = 4\epsilon^2\Gamma$, we can compute the corresponding values of forcing in the model PDE (4) as 0.08140 and 0.04820, which agree well with the values of $F_c = 0.08173$ and $F_d = 0.04811$ found in Figure 3 when we applied AUTO directly to the model PDE.

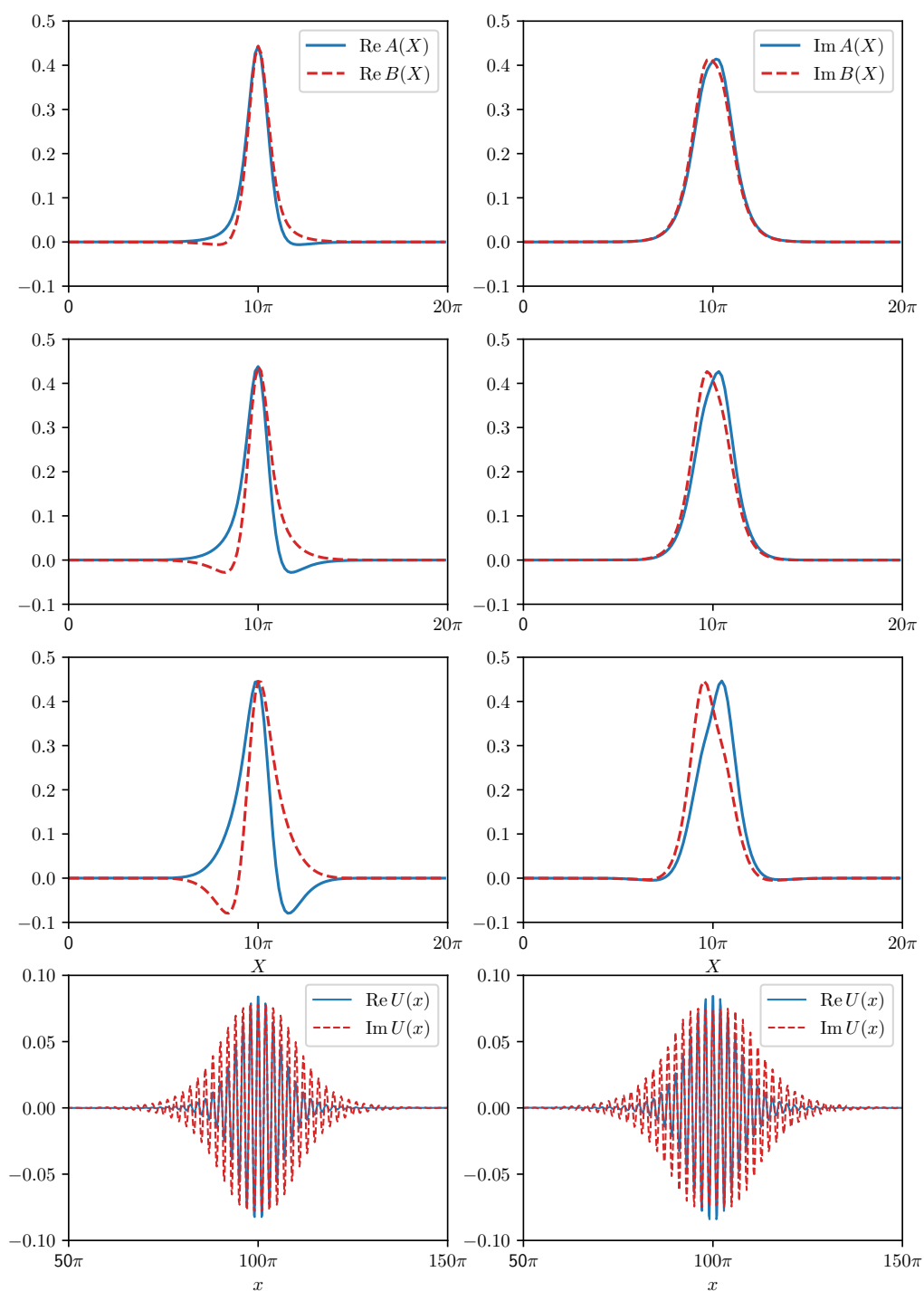


Figure 7. Stationary solutions to the coupled FCGL equations (14) with $\rho = -0.5$, $\nu = 2$, $\alpha = -0.5$, $\beta = 1$, and $C = -1 - 2.5i$. Top row: $v_g = -0.2$ and $\Gamma = 1.46$. Second row: $v_g = -0.5$ and $\Gamma = 1.45$. Third row: $v_g = -1$ and $\Gamma = 1.43$. Bottom row: Approximate solutions $U(x)$ of the PDE model (4) reconstructed from the solutions $A(X), B(X)$ to the coupled FCGL equations assuming $\epsilon = 0.1$; the left and right plots correspond to the top and third rows, respectively.

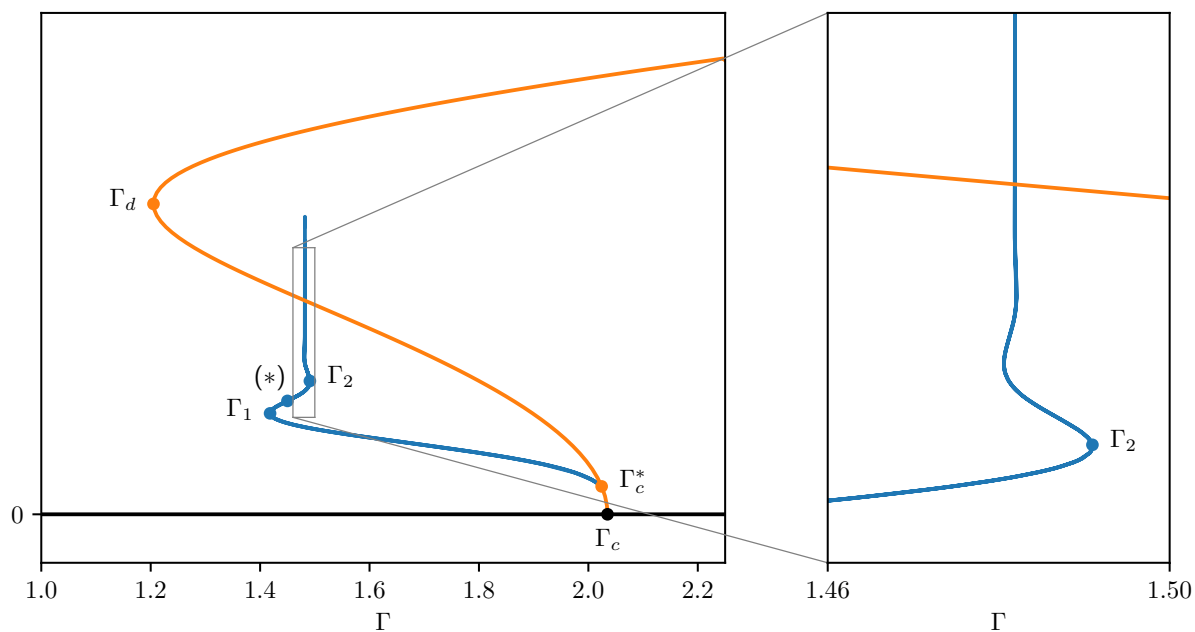


Figure 8. Bifurcation diagram of the coupled FCGL equations with parameters $\rho = -0.5$, $\nu = 2$, $\alpha = -0.5$, $\beta = 1$, $C = -1 - 2.5i$, and $v_g = -0.5$ (corresponding to Figure 3). The bifurcations are at $\Gamma_c = 2.035$, $\Gamma_d = 1.206$, $\Gamma_c^* = 2.024$, $\Gamma_1 = 1.418$, and $\Gamma_2 = 1.491$. The solution marked (*) is shown in the middle row of Figure 7. Numerical results with AUTO suggest that snaking continues beyond Γ_2 , but it is too small to see.

Going back to the coupled FCGL equations, we see a secondary bifurcation at $\Gamma = 2.024$, where a branch of localized solutions bifurcates from the branch of periodic solutions. The localized branch has folds at $\Gamma_1 = 1.418$ and $\Gamma_2 = 1.491$. The corresponding F values in terms of the parameters of the model PDE are 0.05673 and 0.05964, which again agree well with the values of $F_1 = 0.05666$ and $F_2 = 0.05948$ found in Figure 3.

As shown in Figure 8, the localized branch in the bifurcation diagram of the coupled FCGL equations continues to snake upwards after Γ_2 . We believe that these exhibit collapsed snaking, where the saddle-node points asymptote to one value of Γ as one goes up the branch [28]. However, the bifurcation diagram shows that the branch of localized solutions suddenly stops. In fact, AUTO turns around at that point. We believe that this may be caused by AUTO having difficulty handling the phase symmetry in the coupled FCGL equations and that in reality the branch of localized solutions joins with the branch of periodic solutions near the fold at Γ_d , as it does in the bifurcation diagram of the model PDE in Figure 3.

5. Reduction to the real Ginzburg–Landau equation. In this section, we will reduce the coupled FCGL equations to the real Ginzburg–Landau equation close to the subcritical bifurcation from the zero solution to the constant amplitude state. The reduction was done by Riecke [33] in the supercritical case.

We take the complex conjugate of the second equation of (14), so the coupled FCGL equations become

$$(21) \quad \begin{aligned} \frac{\partial A}{\partial T} &= D_1 A + D_2 \frac{\partial^2 A}{\partial X^2} + v_g \frac{\partial A}{\partial X} + C(|A|^2 + 2|B|^2)A + i\Gamma \bar{B}, \\ \frac{\partial \bar{B}}{\partial T} &= \bar{D}_1 \bar{B} + \bar{D}_2 \frac{\partial \bar{B}}{\partial X^2} - v_g \frac{\partial \bar{B}}{\partial X} + \bar{C}(2|A|^2 + |B|^2)\bar{B} - i\Gamma A. \end{aligned}$$

For simplicity, we write

$$(22) \quad D_1 = \rho + i\nu \quad \text{and} \quad D_2 = -2(\alpha + i\beta).$$

In order to reduce the coupled FCGL equation to the real Ginzburg–Landau equation, we apply weakly nonlinear theory close to onset, writing

$$\Gamma = \Gamma_c(1 + \epsilon_2^2 \Gamma_2),$$

where $0 < \epsilon_2 \ll 1$, Γ_c is the critical forcing at critical wavenumber q_c , and Γ_2 is the new bifurcation parameter. We expand the solution in powers of the new small parameter ϵ_2 as follows:

$$\begin{bmatrix} A \\ \bar{B} \end{bmatrix} = \begin{bmatrix} \epsilon_2 A_1 + \epsilon_2^2 A_2 + \epsilon_2^3 A_3 + \cdots \\ \epsilon_2 \bar{B}_1 + \epsilon_2^2 \bar{B}_2 + \epsilon_2^3 \bar{B}_3 + \cdots \end{bmatrix}.$$

From subsection 4.1, the growth rate is real with frequency zero (locked to the forcing), so we scale

$$\frac{\partial}{\partial T} \rightarrow \epsilon_2^2 \frac{\partial}{\partial \tilde{T}}$$

and the preferred wavenumber $q_c \neq 0$, so

$$\frac{\partial}{\partial X} \rightarrow \frac{\partial}{\partial X} + \epsilon_2 \frac{\partial}{\partial \tilde{X}},$$

where \tilde{X} and \tilde{T} are very long space and slow time scales.

At $O(\epsilon_2)$, we have

$$\begin{aligned} 0 &= D_1 A_1 + D_2 \frac{\partial^2 A_1}{\partial X^2} + v_g \frac{\partial A_1}{\partial X} + i\Gamma_c \bar{B}_1, \\ 0 &= \bar{D}_1 \bar{B}_1 + \bar{D}_2 \frac{\partial \bar{B}_1}{\partial X^2} - v_g \frac{\partial \bar{B}_1}{\partial X} - i\Gamma_c A_1. \end{aligned}$$

We can solve the above system by assuming that

$$(23) \quad A_1 = P(\tilde{X}, \tilde{T})e^{iq_c X} \quad \text{and} \quad \bar{B}_1 = Q(\tilde{X}, \tilde{T})e^{-iq_c X}.$$

At this order of ϵ_2 , the coupled FCGL equations become

$$(24) \quad \begin{aligned} 0 &= D_1 P - D_2 q_c^2 P + i v_g q_c P + i\Gamma_c \bar{Q}, \\ 0 &= \bar{D}_1 \bar{Q} - \bar{D}_2 q_c^2 \bar{Q} - i v_g q_c \bar{Q} - i\Gamma_c P. \end{aligned}$$

These can be solved as in subsection 4.1.

Additionally, from the first equation of (24) we get a phase relation between P and Q :

$$(25) \quad \bar{Q} = P e^{i\phi}, \quad \text{where} \quad e^{i\phi} = -\frac{D_1 + i v_g q_c - D_2 q_c^2}{i \Gamma_c}.$$

The fraction in the above equation has modulus 1, so the phase ϕ is real.

At $O(\epsilon_2^2)$, equations (21) become

$$(26) \quad \begin{aligned} 0 &= D_1 A_2 + D_2 \frac{\partial^2 A_2}{\partial X^2} + v_g \frac{\partial A_2}{\partial X} + i \Gamma_c \bar{B}_2 + v_g \frac{\partial A}{\partial \tilde{X}} e^{i q_c X} + 2 i D_2 q_c \frac{\partial A}{\partial \tilde{X}} e^{i q_c X}, \\ 0 &= \bar{D}_1 \bar{B}_2 + \bar{D}_2 \frac{\partial^2 \bar{B}_2}{\partial X^2} - v_g \frac{\partial \bar{B}_2}{\partial X} - i \Gamma_c A_2 - v_g \frac{\partial \bar{B}}{\partial \tilde{X}} e^{i q_c X} + 2 i \bar{D}_2 q_c \frac{\partial \bar{B}}{\partial \tilde{X}} e^{i q_c X}. \end{aligned}$$

At this stage, we would normally define a linear operator in order to impose a solvability condition. In this case, the solvability condition can be deduced directly by setting

$$(27) \quad A_2 = P_2 e^{i q_c X} + \dots \quad \text{and} \quad \bar{B}_2 = \bar{Q}_2 e^{i q_c X} + \dots,$$

where the dots stand for the other Fourier components. This focuses the attention on the $e^{i q_c X}$ component of (26), which is the only component to have an inhomogeneous part and for which the linear operator is singular. Substituting these expressions for A_2 and \bar{B}_2 into (26) and using (25) leads to the following:

$$(28) \quad \begin{bmatrix} D_1 + i v_g q_c - D_2 q_c^2 & i \Gamma_c \\ -i \Gamma_c & \bar{D}_1 - i v_g q_c - \bar{D}_2 q_c^2 \end{bmatrix} \begin{bmatrix} P_2 \\ \bar{Q}_2 \end{bmatrix} + \begin{bmatrix} v_g + 2 i q_c D_2 \\ (-v_g + 2 i q_c \bar{D}_2) e^{i \phi} \end{bmatrix} \frac{\partial P}{\partial \tilde{X}} = \begin{bmatrix} 0 \\ 0 \end{bmatrix},$$

where $e^{i \phi}$ is defined in (25). The square matrix is singular since it is the same one that appears in the linear theory; see (15). We multiply the first line by $i \Gamma_c$ and the second line by $D_1 + i v_g q_c - D_2 q_c^2$, which is effectively the left eigenvector of the matrix, and then add both lines and use (16) and (25), ending up with

$$\left(i \Gamma_c (v_g + 2 i q_c D_2) + \frac{(v_g - 2 i q_c \bar{D}_2)(D_1 + i v_g q_c - D_2 q_c^2)^2}{i \Gamma_c} \right) \frac{\partial P}{\partial \tilde{X}} = 0.$$

Since $\frac{\partial P}{\partial \tilde{X}} \neq 0$, we need

$$- \Gamma_c^2 (v_g + 2 i q_c D_2) + (v_g - 2 i q_c \bar{D}_2)(D_1 + i v_g q_c - D_2 q_c^2)^2 = 0.$$

After substituting (16), we find that this is the same as (17), which is satisfied since q_c is at the minimum of the neutral stability curve.

From the top line of (28), we have the solution

$$\bar{Q}_2 = - \left(\frac{v_g + 2 i q_c D_2}{i \Gamma_c} \frac{\partial A}{\partial \tilde{X}} + \frac{D_1 + i v_g q_c - D_2 q_c^2}{i \Gamma_c} A_2 \right).$$

Thus, we have P_2 arbitrary at this order of ϵ_2 ; we can set $P_2 = 0$, and so, restoring the $e^{i q_c X}$ factor, we have

$$(29) \quad A_2 = 0 \quad \text{and} \quad \bar{B}_2 = -\frac{v_g + 2 i q_c D_2}{i \Gamma_c} \frac{\partial P}{\partial \tilde{X}} e^{i q_c X}.$$

At $O(\epsilon_2^3)$, the problem has the following structure (after using $A_2 = 0$):

$$\begin{aligned}
 \frac{\partial A_1}{\partial \tilde{T}} &= D_1 A_3 + D_2 \frac{\partial^2 A_3}{\partial \tilde{X}^2} + v_g \frac{\partial A_3}{\partial \tilde{X}} + i\Gamma_c \bar{B}_3 \\
 &\quad + D_2 \frac{\partial^2 A_1}{\partial \tilde{X}^2} + i\Gamma_c \Gamma_2 \bar{B}_1 + C(|A_1|^2 + 2|B_1|^2)A_1, \\
 \frac{\partial \bar{B}_1}{\partial \tilde{T}} &= \bar{D}_1 \bar{B}_3 + \bar{D}_2 \frac{\partial^2 \bar{B}_3}{\partial \tilde{X}^2} - v_g \frac{\partial \bar{B}_3}{\partial \tilde{X}} - i\Gamma_c A_3 + 2\bar{D}_2 \frac{\partial^2 \bar{B}_2}{\partial \tilde{X} \partial \tilde{X}} \\
 &\quad - v_g \frac{\partial \bar{B}_2}{\partial \tilde{X}} + \bar{D}_2 \frac{\partial^2 \bar{B}_1}{\partial \tilde{X}^2} - i\Gamma_c \Gamma_2 A_1 + \bar{C}(2|A_1|^2 + |B_1|^2)B_1.
 \end{aligned}
 \tag{30}$$

We focus on the $e^{iq_c X}$ Fourier modes as before and write

$$A_3 = P_3 e^{iq_c X} + \dots \quad \text{and} \quad \bar{B}_3 = \bar{Q}_3 e^{iq_c X} + \dots$$

As at order ϵ_2^2 , we multiply the first equation by $i\Gamma_c$ and the second equation by $D_1 + iv_g q_c - D_2 q_c^2$ and then add them to eliminate P_3 and Q_3 , finding

$$\begin{aligned}
 &i\Gamma_c \frac{\partial A_1}{\partial \tilde{T}} + (D_1 + iv_g q_c - D_2 q_c^2) \frac{\partial \bar{B}_1}{\partial \tilde{T}} \\
 &= i\Gamma_c D_2 \frac{\partial^2 A_1}{\partial \tilde{X}^2} - \Gamma_c^2 \Gamma_2 \bar{B}_1 + i\Gamma_c C(|A_1|^2 + 2|B_1|^2)A_1 \\
 &\quad + 2(D_1 + iv_g q_c - D_2 q_c^2) \bar{D}_2 \frac{\partial^2}{\partial \tilde{X} \partial \tilde{X}} \bar{B}_2 \\
 &\quad - (D_1 + iv_g q_c - D_2 q_c^2) \left(v_g \frac{\partial \bar{B}_2}{\partial \tilde{X}} - \bar{D}_2 \frac{\partial^2 \bar{B}_1}{\partial \tilde{X}^2} \right) \\
 &= i\Gamma_c \Gamma_2 (D_1 + iv_g q_c - D_2 q_c^2) A_1 + \bar{C} (D_1 + iv_g q_c - D_2 q_c^2) (2|A_1|^2 + |B_1|^2) B_1.
 \end{aligned}
 \tag{31}$$

We use (23), (25), and (29) to substitute A_1 , B_1 , and B_2 into the above equation and divide by the common factor of $e^{iq_c X}$. After some manipulation with the help of (16) and (22), this gives the real Ginzburg–Landau equation

$$\begin{aligned}
 \frac{\partial P}{\partial \tilde{T}} &= -\frac{\Gamma_c^2 \Gamma_2}{\rho + 2\alpha q_c^2} P - \frac{4\rho\alpha + 4\nu\beta + v_g^2 + 12v_g\beta q_c + 24(\alpha^2 + \beta^2)q_c^2}{2\rho + 4\alpha q_c^2} \frac{\partial^2 P}{\partial \tilde{X}^2} \\
 &+ 3 \left(C_r + \frac{\nu + v_g q_c + 2\beta q_c^2}{\rho + 2\alpha q_c^2} C_i \right) |P|^2 P.
 \end{aligned}
 \tag{32}$$

Flat solutions of this equation correspond to the simple constant-amplitude solutions discussed in subsection 4.2. The real Ginzburg–Landau equation also has steady sech solutions, so we can find localized solutions of the FCGL equation (14) in terms of hyperbolic functions. The sech solution of (32) is

$$P(\tilde{X}) = \sqrt{\frac{2\Gamma_c^2 \Gamma_2}{h_1}} \operatorname{sech} \left(\sqrt{\frac{\Gamma_c^2 \Gamma_2}{h_2}} \tilde{X} \right) e^{i\phi_1}, \tag{33}$$

where ϕ_1 is an arbitrary phase and

$$\begin{aligned} h_1 &= 3 \left((\rho + 2\alpha q_c^2) C_r + (\nu + v_g q_c + 2\beta q_c^2) C_i \right), \\ h_2 &= -2 \left(\rho\alpha + \nu\beta + \frac{1}{4}v_g^2 + 3v_g\beta q_c + 6(\alpha^2 + \beta^2)q_c^2 \right), \end{aligned}$$

and Γ_2 , h_1 , and h_2 must all have the same sign for the sech solution to exist. From (25), we have $\bar{Q}(\tilde{X}) = P(\tilde{X})e^{i\phi}$.

At leading order,

$$A(X) = \epsilon_2 P(X) e^{iq_c X} = \sqrt{\frac{2\Gamma_c(\Gamma - \Gamma_c)}{h_1}} \operatorname{sech} \left(\sqrt{\frac{\Gamma_c(\Gamma - \Gamma_c)}{h_2}} X \right) e^{i(q_c X + \phi_1)}$$

provided that $\Gamma < \Gamma_c$, $h_1 < 0$, and $h_2 < 0$. Furthermore, (23) and (25) imply that $\bar{B}(X) = A(X)e^{i\phi}$.

Finally, recall that in (5), we wrote the solution to the original PDE (4) as

$$U = \epsilon U_1 = \epsilon \left(A(X, T) e^{ix} + B(X, T) e^{-ix} \right) e^{it}.$$

Substituting the above formulas for A and \bar{B} , we find that

$$U = 2\epsilon \sqrt{\frac{2\Gamma_c(\Gamma - \Gamma_c)}{h_1}} \operatorname{sech} \left(\epsilon \sqrt{\frac{\Gamma_c(\Gamma - \Gamma_c)}{h_2}} x \right) \cos \left((1 + \epsilon q_c)x + \frac{1}{2}\phi + \phi_1 \right) e^{i(t - \frac{1}{2}\phi)}.$$

Using Table 1, we return all parameter values to those used in (4). Thus, we conclude that the spatially localized oscillon is given approximately by

$$(34) \quad U_{loc}(x, t) = \sqrt{\frac{F_c(F - F_c)}{2h_1^*}} \operatorname{sech} \left(\sqrt{\frac{F_c(F - F_c)}{16h_2^*}} x \right) \cos(k_c x + \frac{1}{2}\phi + \phi_1) e^{i(t - \frac{\phi}{2})},$$

where $k_c = 1 + \epsilon q_c$ and h_1^* and h_2^* are given by

$$\begin{aligned} h_1^* &= 3 \left(\mu - \alpha + \gamma + 2\alpha(k_c - 1)^2 \right) C_r \\ &\quad + 3 \left(\omega - \beta + \delta - 1 - 2(\beta - 2\delta)(k_c - 1) + 2\beta(k_c - 1)^2 \right) C_i, \\ h_2^* &= -2\alpha(\mu - \alpha + \gamma) - 2\beta(\omega - \beta + \delta - 1) \\ &\quad - 2(\beta - 2\delta)^2 + 12\beta(\beta - 2\delta)(k_c - 1) - 12(\alpha^2 + \beta^2)(k_c - 1)^2. \end{aligned}$$

This solution U_{loc} gives an approximate oscillon solution of the model PDE (4) valid in the limit of weak dissipation, weak detuning, weak forcing, small group velocity, and small amplitude.

In Figure 9, we compare the asymptotic solution (34), with the localized solution from (4), which we found numerically in section 2. The similarity between the two is quite striking; the main difference is that the real part of the asymptotic solution is somewhat smaller than that of the numerically computed solution, indicating a small error in the phase ϕ .

At this order, we do not find a connection between the position of the sech envelope and that of the underlying $\cos(k_c x)$ pattern. The relative position should not be arbitrary and could presumably be determined using an asymptotic beyond-all-orders theory [11].

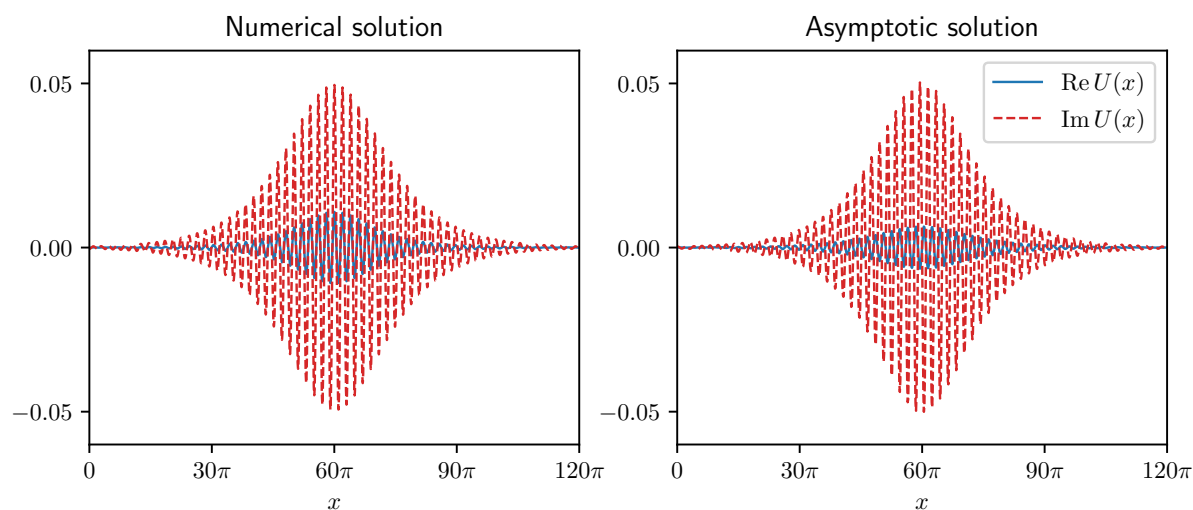


Figure 9. The left panel is the numerical solution of (4), reproduced from Figure 4(c). The right panel shows the asymptotic solution, given in (34). These solutions are at $F = 0.073$.

6. Discussion. In this article, we have shown the existence of oscillons in the PDE (4), which was proposed as a phenomenological model for the Faraday wave experiments in [34]. We first used numerical simulation and found that straightforward time-stepping with carefully chosen parameter values and initial conditions leads to a stable oscillon solution, as shown in Figure 2. We then turned to analysis. Assuming that the damping, detuning, and forcing are weak and that the group velocity and amplitude are small, we reduced the PDE (4) to the coupled FCGL equations (14). We stress that we do not get a single FCGL equation with an \bar{A} term; cf. (3), which is commonly used as a starting point in discussions of oscillons in parametrically forced systems [4, 16, 30]. The single FCGL equation is appropriate when there is a zero-wavenumber bifurcation [2] or if the group velocity is zero. However, if the wavenumber is nonzero (as in Faraday waves) and the group velocity is nonzero but small, the coupled FCGL equations should be used. The coupled FCGL equations and the model PDE both exhibit snaking behavior, though the snaking region is very narrow.

Under the further assumption that the strength of the forcing is close to the onset of instability, we then reduced the coupled FCGL equations to the subcritical real Ginzburg–Landau equation (32). This equation has a sech solution, which, after undoing the reductions, yields an approximate expression for the oscillon; cf. (34). This expression agrees well with the oscillon found numerically (see Figure 9), just as was found in [2], where we studied a zero-wavenumber version of this problem.

One special feature of our model PDE (4) is that the linear terms lead only to positive-frequency oscillations: $U \sim e^{it}$. With spatial dependence, we have left- and right-traveling waves; see (5). In the Faraday wave experiment, as described by the Zhang–Viñals equations [43] or the Navier–Stokes equations [36], the PDEs are real, and so both positive and negative frequency traveling waves can be found. Topaz and Silber [38] wrote down amplitude equations for these traveling waves in the context of two-frequency forcing, without long length scale modulation. In spite of having only positive frequency, our coupled FCGL

equations (with spatial modulation removed) have the same form as the traveling wave amplitude equations in [38] (after truncation to cubic order). These traveling wave equations (without modulation terms) can similarly be reduced to standing wave equations [32, 38] with a phase relationship like (25) between the complex amplitudes of the traveling wave components. Therefore, we expect that the fact that the model PDE (4) has e^{it} dominant should not prevent oscillons being found by the same mechanism in PDEs that are closer to the fluid dynamics because our model PDEs and PDEs for fluid mechanics lead to the same amplitude equation in the absence of spatial modulation.

Since [32, 38] did not include spatial modulations, they did not have to consider the group velocity. In the present study, we assumed that the group velocity is small, of the same order as the amplitude of the solution, in order to make progress. This assumption is questionable in the context of fluid mechanics. It would be better to assume that the group velocity is order one, as in [27]. In that case, the left-traveling wave sees only the average of the right-traveling wave and vice versa, leading to (nonlocal) averaged equations. The authors of [27] found spatially uniform and nonuniform solutions with both simple and complex time dependence but did not study spatially localized solutions. Bringing in spatially localized solutions will be the subject of future work. It is possible to go directly from the PDE (4) to the real Ginzburg–Landau equation [1, 34], and we expect to be able to do a similar reduction for the Zhang–Viñals or the Navier–Stokes equation for fluid mechanics; cf. [36, 43].

In the model PDE (4), when the group velocity is small, waves with a wide range of wavenumbers may be excited. Figure 10 shows two ways in which we can get a fairly small group velocity. The dispersion curve in the left panel is shallow; in this case, many wavenumbers are close to resonant (σ_i is close to 1). Another possibility is to have two resonant wavenumbers around $k = 1$, so that σ_i is close to a minimum (where $v_g = 0$) at $k = 1$; see the right panel for an example. In the latter case, solutions with two nearby wavelengths can be

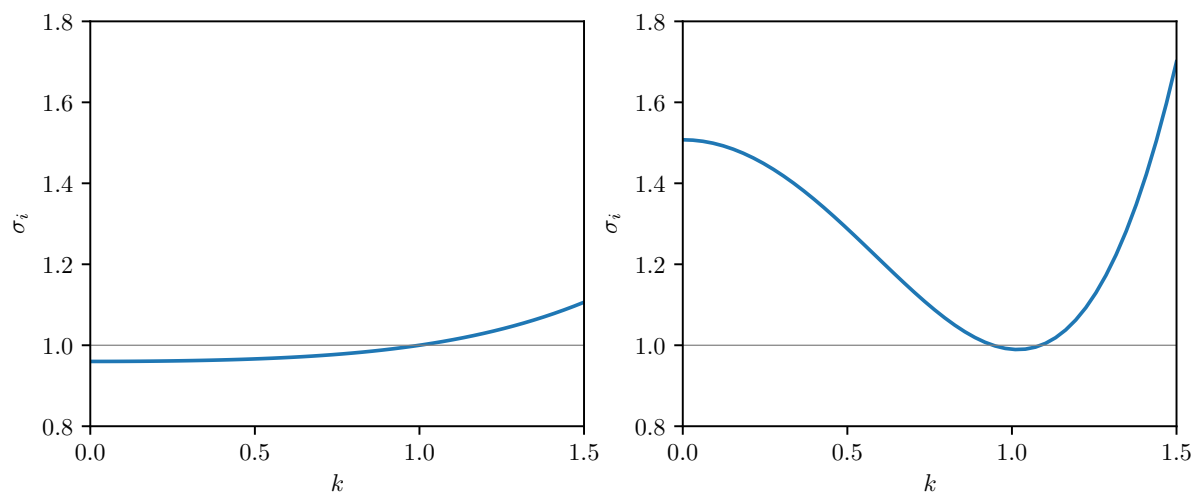


Figure 10. Left panel: The dispersion relation for the PDE model (4) with $\omega = 0.96$, $\beta = -0.02$, and $\delta = 0.02$. The frequency $\sigma_i(k)$ is close to 1 over a wide range of k . Right panel: Dispersion relation for $\omega = 1.5075$, $\beta = 1$, and $\delta = 0.4825$. Now, $\sigma_i(k)$ is equal to 1 at two distinct wavenumbers.

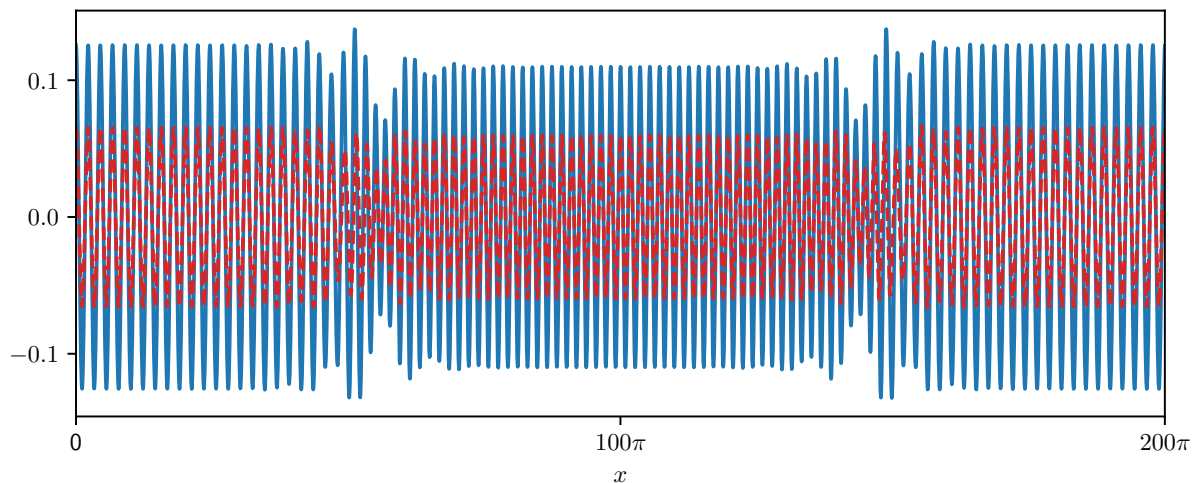


Figure 11. Solution of the PDE model (4) with two wavenumbers. The parameter values are $\mu = -0.255$, $\omega = 1.5075$, $\alpha = -0.5$, $\beta = 1$, $\gamma = -0.25$, $\delta = 0.4825$, $C = -1 - 2.5i$, and $F = 0.15$.

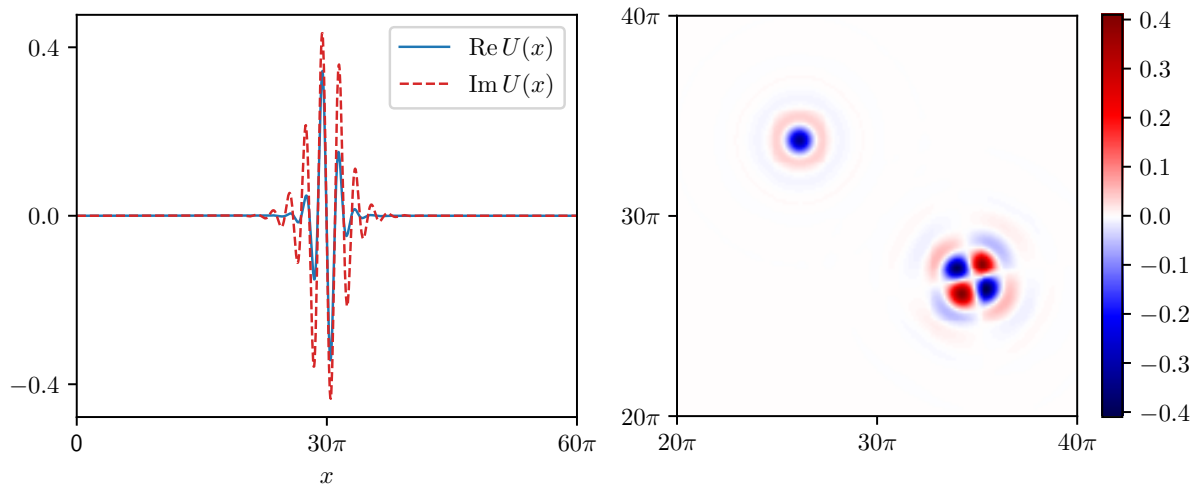


Figure 12. Strongly localized oscillons in the PDE model (4) in one (left) and two (right) dimensions with $\mu = -0.375$, $\omega = 1.99$, $\alpha = -0.5$, $\beta = 1$, $\gamma = -0.25$, $\delta = 0.4975$, $C = -1 - 2.5i$, and $F = 1.5$. The right panel shows the real part of U on only part of the domain $[0, 60\pi] \times [0, 60\pi]$.

expected. Indeed, we did observe such solutions in the PDE model (4); an example is given in Figure 11. These states resemble those found by Bentley [7] in an extended Swift–Hohenberg model and by Riecke [33] in the coupled FCGL equations with small group velocity in the supercritical case.

Finally, we have throughout kept our parameter ϵ small ($\epsilon = 0.1$), which is why the oscillons in, e.g., Figure 4 are so broad, in contrast to the oscillons seen in experiments (see Figure 1). As a preliminary exploration of increasing ϵ , we set $\epsilon = 0.5$, and, after some minor changes to the parameters, we found strongly localized oscillons in one and two dimensions (see Figure 12).

As the picture in two dimensions shows, it is possible for a solution to contain multiple oscillons, which may or may not be axisymmetric. Reference [1] investigates a related PDE: (4) but with strong damping and with cubic-quintic (rather than simply cubic) nonlinearity, where the coefficient of the cubic term has positive real part in order to make the oscillons more nonlinear. In this case, snaking was found in both one and two dimensions.

Acknowledgments. We are grateful for interesting discussions with E. Knobloch and K. McQuighan. We also acknowledge financial support from Al Imam Mohammad Ibn Saud Islamic University.

REFERENCES

- [1] A. S. ALNAHDI, *Oscillons: Localized Patterns in a Periodically Forced System*, PhD thesis, University of Leeds, 2015.
- [2] A. S. ALNAHDI, J. NIESEN, AND A. M. RUCKLIDGE, *Localized patterns in periodically forced systems*, SIAM J. Appl. Dyn. Syst., 13 (2014), pp. 1311–1327.
- [3] I. S. ARANSON AND L. S. TSIMRING, *Domain walls in wave patterns*, Phys. Rev. Lett. 75 (1995), pp. 3273–3276.
- [4] I. S. ARANSON AND L. S. TSIMRING, *Formation of periodic and localized patterns in an oscillating granular layer*, Phys. A, 249 (1998), pp. 103–110.
- [5] H. ARBELL AND J. FINEBERG, *Temporally harmonic oscillons in Newtonian fluids*, Phys. Rev. Lett., 85 (2000), pp. 756–759.
- [6] T. B. BENJAMIN AND F. URSELL, *The stability of the plane free surface of a liquid in vertical periodic motion*, Philos. Trans. R. Soc. Lond. A, 225 (1954), pp. 505–515.
- [7] D. C. BENTLEY, *Localised Solutions in the Magnetorotational Taylor–Couette Flow with a Quartic Marginal Stability Curve*, PhD thesis, University of Leeds 2012.
- [8] C. BIZON, M. D. SHATTUCK, J. B. SWIFT, W. D. MCCORMICK, AND H. L. SWINNEY, *Patterns in 3d vertically oscillated granular layers: Simulation and experiment*, Phys. Rev. Lett., 80 (1998), pp. 57–60.
- [9] J. BURKE AND E. KNOBLOCH, *Homoclinic snaking: Structure and stability*, Chaos, 17 (2007), 037102.
- [10] J. BURKE, A. YOCHELIS, AND E. KNOBLOCH, *Classification of spatially localized oscillations in periodically forced dissipative systems*, SIAM J. Appl. Dyn. Syst., 7 (2008), pp. 651–711.
- [11] S. J. CHAPMAN AND G. KOZYREFF, *Exponential asymptotics of localised patterns and snaking bifurcation diagrams*, Phys. D, 238 (2009), pp. 319–354.
- [12] S. M. COX AND P. C. MATTHEWS, *Exponential time differencing for stiff systems*, J. Comput. Phys., 176 (2002), pp. 430–455.
- [13] C. CRAWFORD AND H. RIECKE, *Oscillon-type structures and their interaction in a Swift–Hohenberg model*, Phys. D, 129 (1999), pp. 83–92.
- [14] J. H. P. DAWES, *Localized pattern formation with a large-scale mode: Slanted snaking*, SIAM J. Appl. Dyn. Syst., 7 (2008), pp. 186–206.
- [15] J. H. P. DAWES, *The emergence of a coherent structure for coherent structures: Localized states in nonlinear systems*, Philos. Trans. R. Soc. Lond. A, 368 (2010), pp. 3519–3534.
- [16] J. H. P. DAWES AND S. LILLEY, *Localized states in a model of pattern formation in a vertically vibrated layer*, SIAM J. Appl. Dyn. Syst., 9 (2010), pp. 238–260.
- [17] S. P. DECENT AND A. D. D. CRAIK, *Hysteresis in Faraday resonance*, J. Fluid Mech., 293 (1995), pp. 237–268.
- [18] E. J. DOEDEL, *AUTO-07P: Continuation and Bifurcation Software for Ordinary Differential Equations*, <https://sourceforge.net/projects/auto-07p> (2012).
- [19] W. S. EDWARDS AND S. FAUVE, *Patterns and quasi-patterns in the Faraday experiment*, J. Fluid Mech., 278 (1994), pp. 123–148.
- [20] M. FARADAY, *On a peculiar class of acoustical figures; and on certain forms assumed by groups of particles upon vibrating elastic surfaces*, Philos. Trans. R. Soc. Lond., 121 (1831), pp. 299–340.
- [21] R. B. HOYLE, *Pattern formation: An introduction to methods*, Cambridge University Press Cambridge, 2006.

- [22] E. KNOBLOCH, *Spatial localization in dissipative systems*, Annu. Rev. Condensed Matter Phys., 6 (2015), pp. 325–359.
- [23] J. LEGA, J. V. MOLONEY, AND A. C. NEWELL, *Swift–Hohenberg equation for lasers*, Phys. Rev. Lett., 73 (1994), pp. 2978–2981.
- [24] O. LIOUBASHEVSKI, H. ARBELL, AND J. FINEBERG, *Dissipative solitary states in driven surface waves*, Phys. Rev. Lett., 76 (1996), pp. 3959–3962.
- [25] O. LIOUBASHEVSKI, Y. HAMIÉL, A. AGNON, Z. RECHES, AND J. FINEBERG, *Oscillons and propagating solitary waves in a vertically vibrated colloidal suspension*, Phys. Rev. Lett., 83 (1999), pp. 3190–3193.
- [26] S. LONGHI, *Spatial solitary waves in nondegenerate optical parametric oscillators near an inverted bifurcation*, Opt. Commun., 149 (1998), pp. 335–340.
- [27] C. MARTEL, E. KNOBLOCH, AND J. M. VEGA, *Dynamics of counterpropagating waves in parametrically forced systems*, Phys. D, 137 (2000), pp. 94–123.
- [28] Y.-P. MA, J. BURKE, AND E. KNOBLOCH, *Defect-mediated snaking: A new growth mechanism for localized structures*, Phys. D, 239 (2010), pp. 1867–1883.
- [29] I. MELBOURNE, *Derivation of the time-dependent Ginzburg–Landau equation on the line*, J. Nonlinear Sci., 8 (1998), pp. 1–15.
- [30] K. MCQUIGHAN AND B. SANDSTEDÉ, *Oscillons in the planar Ginzburg–Landau equation with 2:1 forcing*, Nonlinearity, 27 (2014), pp. 3073–3116.
- [31] V. PETROV, Q. OUYANG, AND H. SWINNEY, *Resonant pattern formation in a chemical system*, Nature, 388 (1997), pp. 655–657.
- [32] J. PORTER AND M. SILBER, *Resonant triad dynamics in weakly damped Faraday waves with two-frequency forcing*, Phys. D, 190 (2004), pp. 93–114.
- [33] H. RIECKE, *Stable wave-number kinks in parametrically excited standing waves*, Europhys. Lett., 11 (1990), pp. 213–218.
- [34] A. M. RUCKLIDGE AND M. SILBER, *Design of parametrically forced patterns and quasipatterns*, SIAM J. Appl. Dyn. Syst., 8 (2009), pp. 298–347.
- [35] M. SHATS, H. XIA, AND H. PUNZMANN, *Parametrically excited water surface ripples as ensembles of oscillons*, Phys. Rev. Lett., 108 (2012), p. 034502.
- [36] A. C. SKELDON AND G. GUIDOBONI, *Pattern selection for Faraday waves in an incompressible viscous fluid*, SIAM J. Appl. Math., 67 (2007), pp. 1064–1100.
- [37] L. TSIMRING AND I. ARANSON, *Localized and cellular patterns in a vibrated granular layer*, Phys. Rev. Lett., 79 (1997), pp. 213–216.
- [38] C. M. TOPAZ AND M. SILBER, *Resonances and superlattice pattern stabilization in two-frequency forced Faraday waves*, Phys. D, 172 (2002), pp. 1–29.
- [39] P. B. UMBANHOWAR, F. MELO, AND H. L. SWINNEY, *Localized excitations in a vertically vibrated granular layer*, Nature, 382 (1996), pp. 793–796.
- [40] J. WU, R. KEOLIAN, AND I. RUDNICK, *Observation of a non-propagating hydrodynamic soliton*, Phys. Rev. Lett., 52 (1984), pp. 1421–1424.
- [41] A. YOCHÉLIS, J. BURKE, AND E. KNOBLOCH, *Reciprocal oscillons and nonmonotonic fronts in forced nonequilibrium systems*, Phys. Rev. Lett., 97 (2006), p. 254501.
- [42] W. ZHANG AND J. VIÑALS, *Secondary instabilities and spatiotemporal chaos in parametric surface waves*, Phys. Rev. Lett., 74 (1995), pp. 690–693.
- [43] W. ZHANG AND J. VIÑALS, *Pattern formation in weakly damped parametric surface waves*, J. Fluid Mech., 336 (1996), pp. 301–330.